ASTROBIOLOGY
Volume 20, Number 8, 2020

DOI: 10.1089/ast.2019.2199

The Radiation Stability of Thymine in Solid H_2O

Christopher K. Materese, Perry A. Gerakines, and Reggie L. Hudson

Abstract

Nucleobases are of significant importance to all known organisms, may be an important building block of life, and could be important biosignatures of current or past life. Given their potential significance to the field of astrobiology, it is important to understand the survival of these molecules when subjected to ionizing radiation as is present in a range of extraterrestrial environments. In this work, we present data on the kinetics of the radiolytic destruction of pure thymine and water + thymine ice mixtures at temperatures from 13 to 150 K. Rate constants were measured using *in situ* infrared spectroscopy, and radiolytic half-lives for thymine were computed for different planetary and interstellar environments. Our results demonstrate that the survival of thymine decreases as the dilution of thymine in water increases. Additionally, we find that thymine survival increases with ice temperature and that this decrease may be related to structure of the ice matrix. Key Words: Nucleobases—Thymine—Ice chemistry—Radiolytic destruction kinetics. Astrobiology 20, 956–963.

1. Introduction

All known life relies on the information encoded in genetic material in the form of RNA or DNA for reproduction and basic cellular function. Despite enormous variations in the forms of life and the extreme range of conditions that can support it, these genetic materials consist of five simple nucleobases. RNA contains the nucleobases adenine (A), guanine (G), cytosine (C), and uracil (U), while DNA includes A, G, and C, but replaces U with thymine (T).

It has been hypothesized that the molecular building blocks of life, including nucleobases, may have origins in the dense interstellar medium (ISM) or in the early solar nebula. Later, these compounds could have been delivered to early Earth via interplanetary dust particles, comets, and/or meteorites (Oró, 1961; Chyba and Sagan, 1992). Indeed, laboratory experiments have demonstrated that nucleobases form abiotically as a product of ice radiation chemistry under conditions similar to those on icy grains in the dense ISM (*e.g.,* Nuevo *et al.,* 2014; Materese *et al.,* 2017, 2018; Oba *et al.,* 2019). Additionally, many *N*-heterocycles including biological and nonbiological nucleobases have been identified in meteorites (*e.g.,* Folsome *et al.,* 1971; Hayatsu *et al.,* 1975; Stoks and Schwartz, 1979; Callahan *et al.,* 2011). Nucleobases may also serve as a potential biosignature and could remain as molecular fossils of ancient organisms under the right conditions. This may be especially relevant in planetary environments such as the surface of Mars or Europa.

We have sought to quantify the stability of nucleobases under conditions relevant to icy planetary and interstellar environments because of their potential importance as both a precursor to, and a remnant of, life. The chemical stability of free nucleobases in liquid water has been studied by Levy and Miller (1998); and, absent any external influence, all but cytosine were shown to have half-lives from 10^6 to 10^8 years at 0°C. Although no published data are available, the stability of nucleobases in water ice at temperatures from 15 to 150 K might be expected to be significantly higher because of the lower temperatures and the absence of a liquid state. The anticipated increased stability of low-temperature molecules in the solid state is a consequence of having fewer individual high-energy collisions and reduced mobility of any potentially reactive species. Under interstellar conditions, and on many planetary surfaces, radiolytic stability may play a significant role in determining the survival of nucleobases.

Previous studies in our lab have quantified the stability of amino acids against ionizing radiation at temperatures from 15 to 140 K (Gerakines *et al.,* 2012; Gerakines and Hudson, 2013, 2015). Amino acids were embedded in ices and subjected to irradiation by 0.8 MeV protons. Infrared spectra of the samples were collected at various stages throughout their irradiation, and changes in band areas as a function of radiation dose were used to quantify reaction kinetics. Room temperature radiolytic destruction of the four bases of DNA (A, C, G, T) using low-energy (30 keV) Ar^+ ions was studied by Huang *et al.* (2014). The radiolysis of room temperature nitrogen heterocycles by exposure to γ rays (^{60}Co), including the canonical nucleobases, was studied by Hammer *et al.* (2019), finding adenine, cytosine, and thymine remarkably

Astrochemistry Laboratory, NASA Goddard Space Flight Center, Greenbelt, Maryland.

resilient with essentially full sample recovery within error at the maximum dosage ($\sim$0.99 MGy). Pilling *et al.* (2011) studied the X-ray photodissociation of uracil and adenine among other compounds. Additionally, the radiolysis (820 MeV Kr^{33+}, 190 MeV Ca^{10+}, 92 MeV Xe^{23+}, 12 MeV C^{4+}) of solid adenine under high vacuum (10^{-8} mbar) at low temperature (13–20 K) has been previously studied by Muniz *et al.* (2017).

In this paper, we present the results of the radiolytic destruction of the nucleobase thymine (Fig. 1) at temperatures relevant to planetary and interstellar environments (13–150 K). These experiments involved the irradiation of micron-thick films of thymine or mixtures of water and thymine for a range of relative abundances and temperatures. The methods we used were similar to those of Gerakines *et al.* (2012) and Gerakines and Hudson (2013, 2015), in that infrared spectra were collected after various irradiation doses to monitor changes and quantify the kinetics of the radiolysis. We have also used these data to determine the half-lives of thymine in a number of extraterrestrial environments.

2. Experimental Methods

Experiments were performed in a high-vacuum chamber evacuated by a turbomolecular pump to a pressure of a few 10^{-7} torr. For a detailed schematic of our vacuum chamber and associated instruments, see Gerakines *et al.* (2012). Samples were deposited on a polished aluminum substrate (area $\approx 5\,cm^2$) mounted on a rotatable closed-cycle helium cryocooler inside the vacuum chamber. The temperature of the substrate was monitored by a silicon diode sensor and controlled with a resistive heater and PID controller. The vacuum chamber was interfaced to an IR spectrometer (Nicolet Nexus 670 FT-IR) and attached to the beamline of a Van de Graaff accelerator. The IR beam was reflected off the polished substrate at a near-normal angle, and spectra were collected with a cooled HgCdTe (MCT) detector. All IR spectra were 100-scan averages with a resolution of $2\,cm^{-1}$ from 5000 to $650\,cm^{-1}$.

A Knudsen-type sublimation oven was used for nucleobase deposition. This oven consisted of a copper block with a small cavity ($\approx 0.05\,cm^3$) underneath a copper plate that was bolted to the top with a $\sim$1 mm diameter hole centered over the cavity. The block was held in thermal contact with a 100 Ω resistive heater connected to a 20 V, 225 mA DC power supply. The temperature of the oven was monitored by a diode sensor and regulated by a PID temperature controller ($T_{max} \approx 300$°C). The opening of the oven was positioned approximately 5 cm from the substrate and a baffle placed between the opening and the substrate to minimize contamination of the rest of the vacuum system.

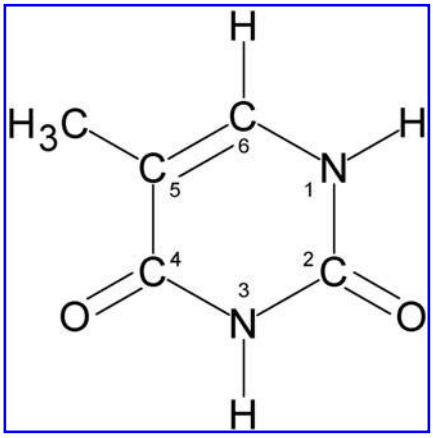

FIG. 1. The structure of thymine.

Thymine (solid; Sigma, ≥99% purity) was heated in the oven to 185°C, which was sufficient for a reasonable sublimation rate without causing thermal decomposition. Preliminary experiments were performed to calibrate the deposition rate of thymine onto the substrate at this temperature. Water (liquid; Fisher HPLC grade) was freeze-pump-thawed three times to remove excess dissolved gases and then vapor deposited via a capillary tube. The H_2O deposition rate was controlled by metered leak valves, which were calibrated over a wide range of settings in order to provide the desired ice compositions. In this study, we created samples of thymine, and H_2O + thymine in ratios of approximately 1:1, 10:1, and 50:1. Samples were grown at 150, 100, 50, or 13 K. For most experiments, the temperature of the ice during proton irradiation was the same as for the sample growth; however, a few experiments were performed in which the mixtures were created at 100 K and irradiation was carried out at 20 K. All samples were approximately 1 μm thick, as determined by measuring the interference fringes from a laser reflected from the sample surface during deposition. Experiments typically lasted for 5–6 h, and some condensation of residual gases in the vacuum system (mostly H_2O) is expected (at or below the 1% level). Condensation of these gases will not have a significant effect on the radiation chemistry, the calculated irradiation doses, or IR spectra over the course of a single experiment.

Ice irradiation was performed by bombarding the sample with a beam of 0.8–1.0 MeV protons at a current of $\sim 1.5\times10^{-7}$ A. To perform an irradiation, the substrate was rotated to face the proton beam. After each irradiation step, the substrate was rotated 180° for collection of IR spectra, then returned to the previous position for further radiation doses if required. The doses absorbed by the samples were computed by using the following formulas and are summarized in Table 1:

$$\mathrm{Dose(MGy)} = SF \times \left(1.602 \times 10^{-22}\right) \tag{1a}$$

$$\mathrm{Dose}\left(\mathrm{eVmolec}^{-1}\right) = m_{\mathrm{avg}} SF \tag{1b}$$

Table 1. Properties of Thymine and Mixed H_2O + Thymine Ice Mixtures and Interactions with Assuming 0.9 MeV Protons

Sample (H_2O:Thymine)	Stopping power, S [eV cm^2 g^{-1} p^{+-1}]	Average molar mass [g mol^{-1}]	Average density [g cm^{-3}]
0:1	2.54×10^8	126.11	1.23
1:1	2.56×10^8	72.06	1.08
10:1	2.62×10^8	27.84	0.948
50:1	2.66×10^8	20.13	0.926

Here, S is the proton stopping power (eV cm^2 g^{-1} p^{+-1}), F is the incident proton fluence (p$^+$ cm^{-2}), and m_{avg} is the average mass per molecule of the sample. The proton stopping power (assuming an energy of 0.9 MeV) for each sample was calculated from the Stopping and Range of Ions in Matter (SRIM) software (Ziegler *et al.,* 2010). The densities of single component thymine samples were assumed to be the same as the room temperature density, while the densities of water + thymine mixtures were assumed to be the average of their densities, weighted by their relative abundances.

3. Results

The destruction of thymine was measured in samples of thymine and H_2O + thymine (1:1, 10:1, and 50:1). The IR spectra of the samples as created and at various irradiation doses are shown in Fig. 2. Changes in the IR spectra due to the destruction of thymine and the formation of products are evident. Here, we focus primarily on the kinetics of the thymine destruction, rather than the identification of new products. Nonetheless, we were able to easily identify several products that are consistent with the breakup of the thymine molecule: CO (at 2137 cm^{-1}), CO_2 (at 2342 cm^{-1}), $^{13}CO_2$ (at 2275 cm^{-1}), OCN^- (at 2170 cm^{-1}), and HNCO (at 2252 cm^{-1}).

The proton irradiation of thymine-containing ices is expected to give a large number of stable reaction products, but only the simplest can be identified by our *in situ* methods. However, our solid-phase experiments do have the advantage of leading to the unequivocal conclusion that the products identified are indeed formed in the ice sample, as opposed to being produced or found only after some type of warming for a liquid- or gas-phase analysis. As for specifics, thymine's structure possesses two H, N, C, O sequences, so it is not surprising that isocyanic acid (H-N=C=O) is a radiolytic degradation product. Irradiation of HNCO, in turn, can explain the CO observed, and our own experience is that CO_2 follows from most any observation of CO. Among the simpler ways to make carbon dioxide is the well-known reaction of CO with hydroxyl radicals, OH + CO → CO_2 + H. Elimination of CO from the parent molecule also is a possible source of CO. Since any HNCO formed will be in the presence of thymine, a base, then proton transfer to produce OCN^- is not surprising, and accounts for the cyanate ion seen in our spectra (~2170 cm^{-1}). If a thymine molecule can fragment to give HNCO, then one might also expect to see methyl acetylene (propyne, HC≡C-CH_3), but the overlap of that molecule's strongest IR features with those of our reactants is too severe for any firm identification.

Beyond these simple considerations concerning reaction chemistry, there is a large and evolving literature on the reactions of nucleobases with both prehydrated (''dry'') and hydrated (''wet'') secondary electrons. Density functional calculations show that the electron affinity of thymine is the

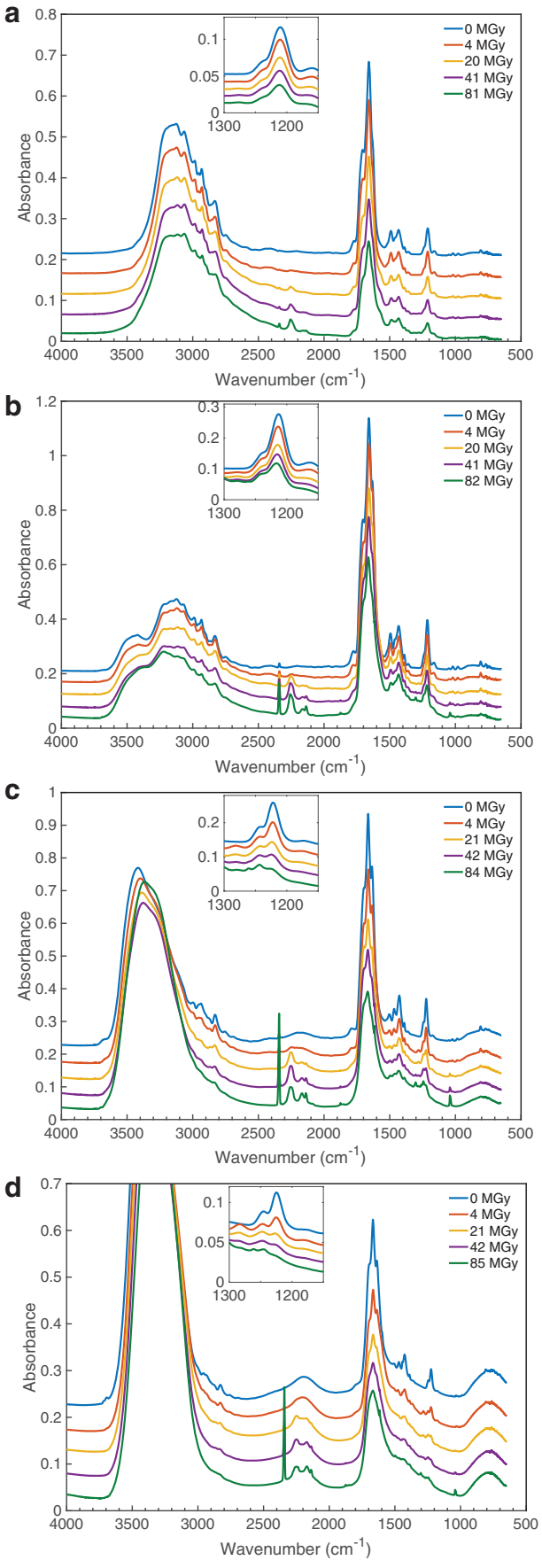

FIG. 2. The IR spectra of thymine and H_2O + thymine mixtures before and after exposure to radiation at the specified doses: (**a**) thymine, (**b**) H_2O + thymine (1:1) mixture, (**c**) H_2O + thymine (10:1) mixture, (**d**) H_2O + thymine (50:1) mixture. Insets are magnifications of the 1222 cm^{-1} band. Color images are available online.

highest, or close to highest, of the four DNA nucleobases (Li *et al.*, 2002), and laboratory observations show that thymine has the greatest reactivity with prehydrated electrons (Ma *et al.*, 2017). For reactions of thymine with low-energy electrons see Boudaïffa *et al.* (2000), and for the older literature involving oxidation-reduction and nucleobase irradiations see Box (1977).

The kinetics of thymine destruction was quantified by measuring changes in integrated areas of a chosen thymine band, which were assumed to be proportional to the number of thymine molecules per unit area in the sample. Specifically, an IR band centered at approximately 1211 cm^{-1} (and approximately 1222 cm^{-1} in a water matrix; see Fig. 2), corresponding to a ring stretch + C6-H in-plane bending mode (Nowak, 1989), was selected to track the destruction of thymine because of its minimal overlap with absorptions due to H_2O. Since the band is part of a larger feature, the entire feature was fit by using two (or three when needed to account for the growth of a product late in the irradiation) Gaussian curves to isolate it from neighboring bands (see Fig. 3).

Destruction of thymine was tracked by monitoring the ratio of the band area A after an irradiation dose D to the band's initial area A_0, before irradiation. Similar to our previous work with amino acids (see, *e.g.,* Gerakines *et al.*, 2012; Gerakines and Hudson, 2013, 2015) and the work on the destruction of adenine by Muniz *et al.* (2017), trends of A/A_0 versus D reflect an exponential decay, suggesting approximately first-order kinetics. For this analysis we assumed

$$\text{thymine} \rightleftharpoons \text{products} \tag{2}$$

for thymine destruction with both forward and backward reactions assumed to be first order. Thymine decay data were fit to the equation

$$(A/A_0) = ae^{-bD} + c \tag{3}$$

which represents the fraction of thymine molecules remaining in the sample after radiation dose D. As discussed by Gerakines and Hudson (2015), parameter a is the fractional loss of thymine after high radiation doses, b is equal to the sum of the forward and backward rate constants in Eq. 3, and c is the equilibrium fraction of thymine. The thymine decay data and corresponding best-fit exponential curves are shown in Fig. 4 with fitting parameters summarized in Table 2.

The forward destruction-rate constant k was determined from the curve-fitting parameters (where $k = ab$), and the half-life doses were computed from the decay curves (Table 3). Note, no attempt was made to extrapolate half-lives beyond the doses recorded. Additionally, radiation chemical yields G(-thy), frequently used by radiation chemists, were computed for all experimental samples and are also summarized in Table 3. A detailed explanation of the calculation of G values is given by Gerakines *et al.* (2012). While the decay data in each experiment can be reasonably well fit by an exponential curve and roughly conform to first-order kinetics, we note that the goodness of the fits decreases when H_2O is included in the sample (see Fig. 4, Table 2). This could be caused by an increased complexity of the chemistry between H_2O and thymine such that the first-order kinetics reflected in Eq. 3 may be too simple to describe it.

Most samples were irradiated at the same temperature at which they were created, but an additional series of experiments was also performed to better understand the effects of deposition temperature. In these experiments, sample ices were created at 100 K and then cooled to 20 K for irradiation. Data from these experiments were modeled by the same procedure as in all previous experiments. The destruction rate constants obtained are compared to those from experiments where samples were created and irradiated at the same temperatures in Fig 5.

4. Discussion

The destruction rate constant of thymine generally increases as the initial ratio of water to thymine increases (see Table 3, Fig. 5). This demonstrates that a greater relative abundance of H_2O causes a greater fractional destruction of thymine for a given radiation dose. This effect may be influenced by various factors: for example, reactive species produced in the water may contribute to the destruction of

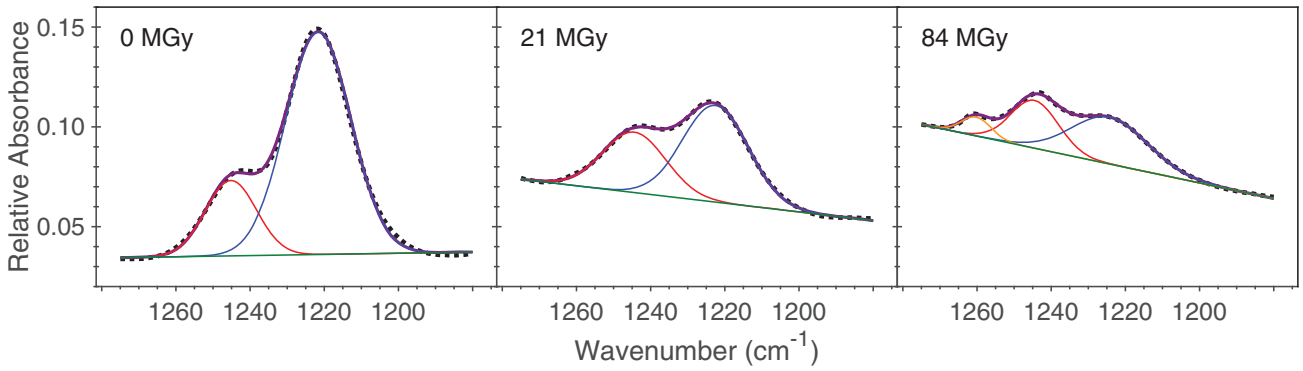

FIG. 3. Examples of fitting the feature containing the 1222 cm^{-1} band, using spectra from the H_2O + thymine (10:1) experiment at 13 K. The dotted line in each case represents the measured spectrum. The purple curve in each case represents the sum of the Gaussian functions chosen to fit the spectrum. Two Gaussian functions (in red and blue) were sufficient to reproduce most spectra, with a third (in orange) needed after large doses (likely due to an unidentified product of the irradiation). The area of the blue Gaussian curve after each irradiation step is used to track the decomposition of thymine with dose, as displayed in Fig. 4. Color images are available online.

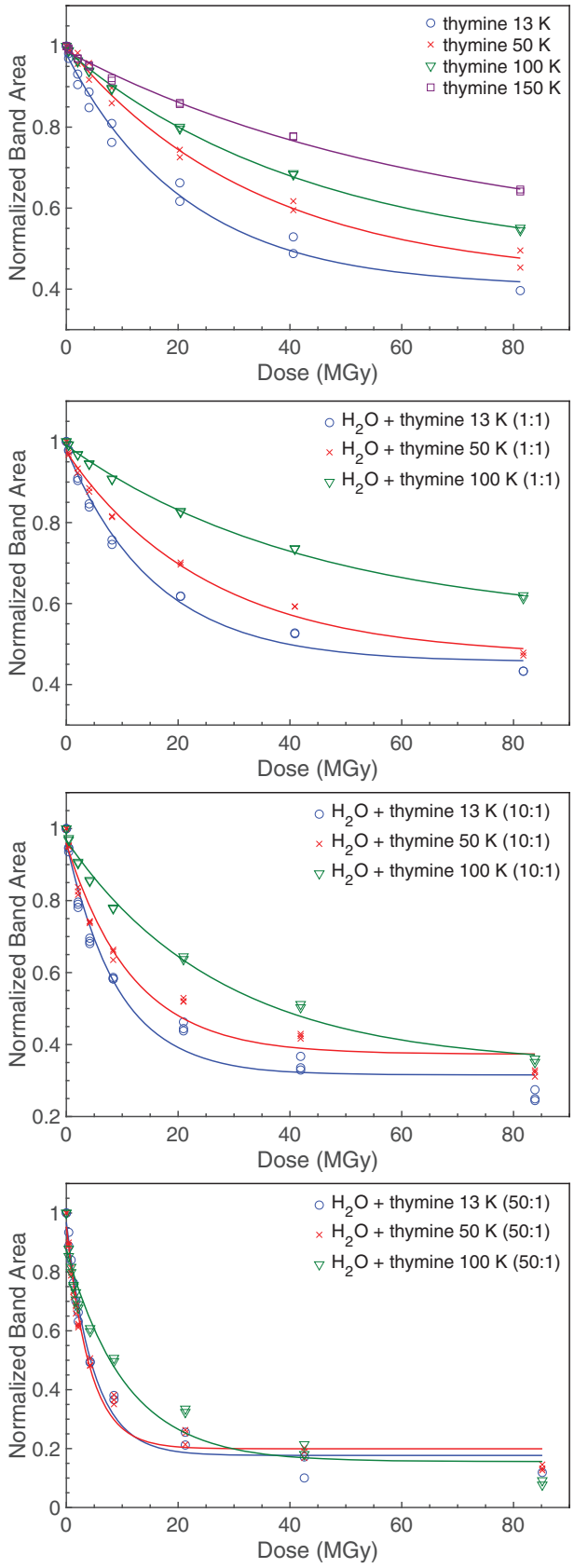

FIG. 4. Thymine decay data for all samples overlaid with best-fitting exponential curves of the form of Eq. 3. Color images are available online.

neighboring thymine molecules. In addition to serving as a potential reactant, H_2O has also been demonstrated to act as a proton acceptor, enhancing radiolytic reactions in ices. Both of these factors just listed could be responsible for an increase in k but would likely taper off after thymine molecules are effectively matrix isolated. Because large bands from an H_2O matrix can obscure small bands of dilute thymine mixtures, we are experimentally limited by our ability to measure changes in the IR bands of thymine, and this work did not attempt to reach a state of true matrix isolation to observe this.

The temperatures of the samples also affected the value of the rate constant k. For almost all samples, k decreased as the temperature increased (Table 3, Fig. 6). This result is somewhat counterintuitive since an increase in temperature often leads to an increase in reaction rate, but it may be partially explained by differences in the structure of the surrounding matrix since ices created at 13 K are likely to be more amorphous in nature than those created at 100 K.

In the additional series of experiments described above (in which all samples were deposited at 100 K and then irradiated at 20 K), the values of k were found to be lower relative to those obtained from experiments where the samples were deposited and irradiated at 13 K. Although within the margin of error, these k values were still slightly elevated relative to those obtained from experiments where the samples had been deposited and irradiated at 100 K (Fig 7). We hypothesize that thymine may be better segregated in more crystalline ices than in more amorphous ices, leading in part to the differences observed in k.

The half-lives of thymine in a range of Solar System and interstellar conditions are summarized in Table 4. These half-lives were obtained by using the radiation dose rates at the given object and the data from our experiments at the nearest appropriate temperature. We note that these half-lives should be considered rough estimates when outside a laboratory setting. This is because these experiments used simplified pure and two-component mixtures and likely have a much greater relative abundance of thymine than would be expected in ices found in actual space environments. High-radiation environments like Europa would lose thymine (<0.1% of the initial sample remaining) in timescales on the order of 10 years at the surface, 1000 to 10,000 years at a depth of 1 cm, and 10^7 to 10^8 years at a depth of 1 m. On Kuiper Belt Objects like Pluto, thymine could survive on timescales of hundreds of millions of years at a depth of 1 μm and billions of years at a depth of 1 cm. In comets, thymine could survive in timescales of millions to tens of millions of years at a depth of 1 μm and billions of years at a depth of 1 cm.

5. Astrobiological Implications

Understanding the kinetics of the radiolytic destruction of nucleobases and other potential biosignatures is important in our search for life elsewhere in the Solar System. Should thymine-utilizing life exist in an environment such as the subsurface ocean of Europa, it is important to know how long remnant biosignatures could survive should they be brought near the surface through resurfacing events. The age of the surface of Europa is approximately 10^7 years as

TABLE 2. CURVE FIT PARAMETERS FOR THE RADIOLYTIC DECAY OF THYMINE

Sample	T [K]	Curve fit parameters—functional form: $ae^{-bD} + c$		
		a	b [MGy^{-1}]	c
Thymine	13	0.58 ± 0.03	0.046 ± 0.006	0.40 ± 0.03
	50	0.58 ± 0.02	0.029 ± 0.003	0.42 ± 0.02
	100	0.52 ± 0.01	0.022 ± 0.001	0.47 ± 0.02
	150	0.48 ± 0.04	0.015 ± 0.002	0.51 ± 0.04
H_2O + thymine (1:1)	13	0.52 ± 0.02	0.063 ± 0.006	0.46 ± 0.02
	50	0.51 ± 0.02	0.040 ± 0.004	0.47 ± 0.02
	100	0.44 ± 0.02	0.023 ± 0.002	0.55 ± 0.02
H_2O + thymine (10:1)	13	0.65 ± 0.02	0.11 ± 0.01	0.32 ± 0.2
	50	0.59 ± 0.02	0.085 ± 0.01	0.37 ± 0.02
	100	0.63 ± 0.03	0.036 ± 0.004	0.34 ± 0.03
H_2O + thymine (50:1)	13	0.79 ± 0.03	0.21 ± 0.02	0.18 ± 0.02
	50	0.75 ± 0.02	0.24 ± 0.02	0.20 ± 0.01
	100	0.72 ± 0.04	0.094 ± 0.017	0.16 ± 0.03

TABLE 3. RADIATION CHEMICAL YIELDS, DESTRUCTION RATE CONSTANTS, AND HALF-LIVES FOR THYMINE IN DIFFERENT ICE MIXTURES AND TEMPERATURES

Sample	T [K]	G(-thy) [molec $(100\ ev)^{-1}$]	Destruction rate constant k [MGy^{-1}]	Half-life dose [MGy]
Thymine	13	2.0 ± 0.3	0.027 ± 0.007	38 ± 3
	50	1.3 ± 0.1	0.017 ± 0.004	69 ± 3
	100	0.90 ± 0.06	0.012 ± 0.002	>80
	150	0.56 ± 0.10	0.0073 ± 0.003	>80
H_2O + thymine (1:1)	13	2.2 ± 0.2	0.033 ± 0.007	41 ± 2
	50	1.3 ± 0.1	0.020 ± 0.004	71 ± 3
	100	0.66 ± 0.06	0.010 ± 0.002	>80
H_2O + thymine (10:1)	13	2.2 ± 0.3	0.069 ± 0.014	12 ± 1
	50	1.6 ± 0.2	0.050 ± 0.012	18 ± 1
	100	0.72 ± 0.09	0.023 ± 0.005	38 ± 3
H_2O + thymine (50:1)	13	1.5 ± 0.2	0.16 ± 0.03	4.3 ± 0.5
	50	1.7 ± 0.1	0.18 ± 0.03	3.8 ± 0.2
	100	0.64 ± 0.12	0.068 ± 0.02	8.0 ± 1.6

estimated by cratering (Zahnle *et al.*, 2003). Depending on the accuracy of the estimate, our results suggest that at a depth of 1 m for a H_2O + thymine (50:1) mixture, thymine should have undergone between 0.6 and 6 half-lives over that period (meaning 2–70% of the original thymine would remain).

Radiolytic destruction kinetics are also important for our understanding of the potential abiotic origins of nucleobases. Our current work suggests that, for example, should thymine form on icy grains in a dense molecular cloud, as suggested in the works of Materese *et al.* (2013) and Oba *et al.* (2019), it would have a destruction half-life on the order of 10^4 to 10^5

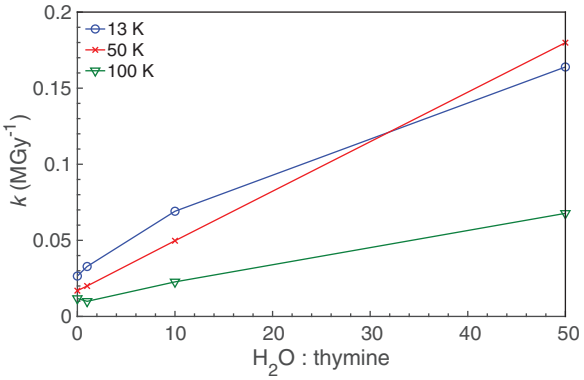

FIG. 5. Thymine destruction rate constant k as a function of H_2O:thymine. Color images are available online.

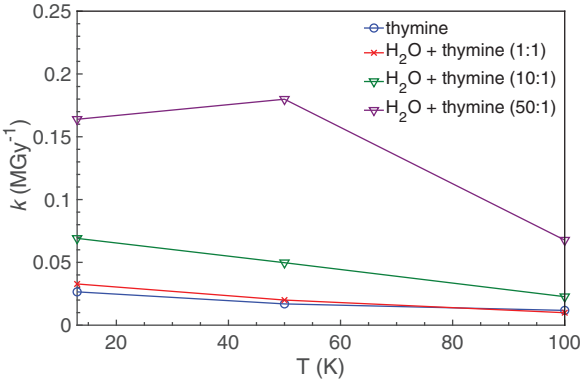

FIG. 6. Thymine destruction rate constant k as a function of temperature (deposition and irradiation). Color images are available online.

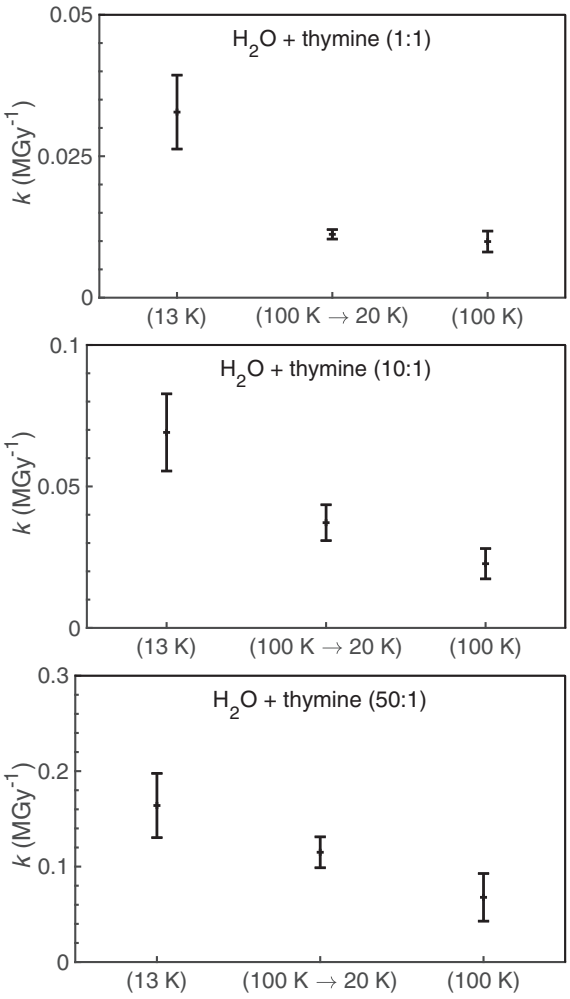

FIG. 7. The effect of deposition temperature on thymine destruction rate constants (k). Each panel shows the k value obtained for experiments where the ices were deposited and irradiated at 13 K (left), deposited at 100 K but irradiated at 20 K (middle), and deposited and irradiated at 100 K (right).

years, which is shorter than the expected lifetime of the cloud itself. This relatively short half-life may contribute to the lack of detection of thymine in meteoritic samples. Notably, the half-life of pure thymine in a dense cloud determined here is shorter than that of pure adenine (10^6 to 10^7 years) as determined by Muniz *et al.* (2017). The differences in half-lives between adenine and thymine are not inconsistent with the results of Huang *et al.* (2014), which determined that thymine is degraded significantly faster than adenine under room temperature low-energy radiolysis. In the case of objects such as comets, thymine accreted into comets would not significantly survive at depths of 1 cm or less but would survive at greater depths.

6. Conclusion

We have measured the radiolytic destruction of thymine and thymine in mixed H_2O + thymine ices over a range of temperatures relevant to the Solar System and interstellar space. The destruction rate constant k of thymine increases with a decreasing concentration of thymine in our H_2O + thymine samples. Additionally, k generally decreases with increasing temperature of the ice. Much of the temperature dependence of k seems to be related to the initial deposition temperature of the ice, suggesting that the structure of the ice lattice may play an important role in modulating this value. Our results suggest that thymine is best preserved under conditions where it is most highly concentrated and where any ice matrix is more highly crystalline. In contrast, it is least preserved under highly dilute conditions with a more amorphous ice matrix.

Acknowledgments

This work was supported by the National Aeronautics and Space Administration through the NASA Exobiology Program, the Goddard Center for Astrobiology, and the FLaRe ISFM at Goddard. We thank Steve Brown and Eugene Gerashchenko of the Radiation Effects Facility at NASA Goddard Space Flight Center for the operation of the Van de Graaff accelerator.

Table 4. Estimated Thymine Half-Lives in Planetary and Interstellar Environments

Location	T [K]	Depth [cm]	Dose rate [Gy yr^{-1}]	Half-life [yr] Thymine	H_2O + thymine (1:1)	H_2O + thymine (10:1)	H_2O + thymine (50:1)
Europa[a]	100	10^{-3}	$18.\times10^{7}$	-	-	$2.1\pm0.2\times10^{0}$	$4.4\pm0.9\times10^{-1}$
		1	1.2×10^{4}	-	-	$3.2\pm0.3\times10^{3}$	$6.8\pm1.4\times10^{2}$
		100	1.7×10^{0}	-	-	$2.2\pm0.2\times10^{7}$	$4.7\pm0.9\times10^{6}$
Pluto[b]	40	10^{-4}	1.2×10^{-1}	$5.9\pm0.3\times10^{8}$	$6.1\pm0.3\times10^{8}$	$1.5\pm0.1\times10^{8}$	$3.3\pm0.2\times10^{7}$
		100	3.5×10^{-2}	$2.0\pm0.1\times10^{9}$	$2.0\pm0.1\times10^{9}$	$5.2\pm0.3\times10^{8}$	$1.1\pm0.1\times10^{8}$
Comets[c]	40	10^{-4}	5.4×10^{0}	$1.3\pm0.1\times10^{7}$	$1.3\pm0.1\times10^{7}$	$3.4\pm0.2\times10^{6}$	$7.1\pm0.4\times10^{5}$
		1	4.1×10^{-2}	$1.7\pm0.1\times10^{9}$	$1.7\pm0.1\times10^{9}$	$4.4\pm0.2\times10^{8}$	$9.2\pm0.5\times10^{7}$
Diffuse[d] ISM	40	-	5.4×10^{5}	$7.1\pm0.5\times10^{1}$	$7.7\pm0.4\times10^{1}$	$2.2\pm0.2\times10^{1}$	$8.0\pm0.9\times10^{0}$
Dense[d] ISM	10	-	1.1×10^{2}	$3.5\pm0.3\times10^{5}$	$3.8\pm0.2\times10^{5}$	$1.1\pm0.1\times10^{5}$	$4.0\pm0.5\times10^{4}$

Original data sources:
[a]Paranicas *et al.* (2009), dose rate includes protons and electrons.
[b]Hudson *et al.* (2008).
[c]Strazzulla *et al.* (2003).
[d]Moore *et al.* (2001), dose includes protons and UV photons.
ISM = interstellar medium.

References

Boudaïffa, B., Cloutier, P., Hunting, D., Huels, M.A., and Sanche, L. (2000) Resonant formation of DNA strand breaks by low-energy (3 to 20 eV) electrons. *Science* 287:1658–1660

Box, H.C. (1977) *Radiation Effects: ESR and ENDOR Analysis*, Academic Press, New York.

Callahan, M.P., Smith, K.E., Cleaves, H.J., II, Ruzicka, J., Stern, J.C., Glavin, D.P., House, C.H., and Dworkin, J.P. (2011) Carbonaceous meteorites contain a wide range of extraterrestrial nucleobases. *Proc Natl Acad Sci USA* 108: 13995–13998.

Chyba, C. and Sagan, C. (1992) Endogenous production, exogenous delivery and impact-shock synthesis of organic molecules: an inventory for the origins of life. *Nature* 355: 125–132.

Folsome, C.E., Lawless, J., Romiez, M., and Ponnamperuma, C. (1971) Heterocyclic compounds indigenous to the Murchison meteorite. *Nature* 232:108–109.

Gerakines, P.A. and Hudson, R.L. (2013) Glycine's radiolytic destruction in ices: first *in situ* laboratory measurements for Mars. *Astrobiology* 13:647–655.

Gerakines, P.A. and Hudson, R.L. (2015) The radiation stability of glycine in solid CO_2—*in situ* laboratory measurements with applications to Mars. *Icarus* 252:466–472.

Gerakines, P.A., Hudson, R.L., Moore, M.H., and Bell, J.-L. (2012) *In situ* measurements of the radiation stability of amino acids at 15–140 K. *Icarus* 220:647–659.

Hammer, P.G., Yi, R., Yoda, I., Cleaves, J.C., II, and Callahan, M.P. (2019) Radiolysis of solid-state nitrogen heterocycles provides clues to their abundance in the early Solar System. *Int J Astrobiol* 18:289–295.

Hayatsu, R., Anders, E., Studier, M.H., and Moore, L.P. (1975) Purines and triazines in the Murchison meteorite. *Geochim Cosmochim Acta* 39:471–488.

Huang, Q., Su, X., Yoa, G., Lu, Y., Ke, Z., Liu, J., Wu, Y., and Yu, Z. (2014) Quantitative assessment of the ion-beam irradiation induced direct damage of nucleic acid bases through FTIR spectroscopy. *Nucl Instrum Methods Phys Res B* 330: 47–54.

Hudson, R.L., Palumbo, M.E., Strazzulla, G., Moore, M.H., Cooper, J.F., and Sturner, S.J. (2008) Laboratory studies of the chemistry of trans-Neptunian object surface materials. In *The Solar System Beyond Neptune,* edited by M.A. Barucci, H. Boehnhardt, D.P. Cruikshank, and A. Morbidelli, University of Arizona Press, Tucson, AZ, pp 507–523.

Levy, M. and Miller, S. (1998) The stability of RNA bases: implications for the origin of life. *Proc Natl Acad Sci USA* 95:7933–7938.

Li, C., Cai, A., and Sevilla, M.D. (2002) DFT calculations of the electron affinities of nucleic acid bases: dealing with negative electron affinities. *J Phys Chem A* 106:1596–1603.

Ma, J., Wang, F., Denisov, S.A., Adhikary, A., and Mostafavi, M. (2017) Reactivity of prehydrated electrons toward nucleobases and nucleotides in aqueous solution. *Sci Adv* 3, doi: 10.1126/sciadv.1701669.

Materese, C.K., Nuevo, M., Bera, P.P., Lee, T.J., and Sandford, S.A. (2013) Thymine and other prebiotic molecules produced from the ultraviolet photo-irradiation of pyrimidine in simple astrophysical ice analogs. *Astrobiology* 13:948–962.

Materese, C.K., Nuevo, M., and Sandford, S.A. (2017) The formation of nucleobases from the ultraviolet photoirradiation of purine in simple astrophysical ice analogs. *Astrobiology* 17:761–770.

Materese, C.K., Nuevo, M., McDowell, B.L, Buffo, C.E., and Sandford, S.A. (2018) The photochemistry of purine in ice analogs relevant to dense interstellar clouds. *Astrophys J* 864, doi:10.3847/1538-4357/aad328.

Moore, M.H., Hudson, R.L., and Gerakines, P.A. (2001) Mid- and far-infrared spectroscopic studies of the influence of temperature, ultraviolet photolysis and ion irradiation on cosmic-type ices. *Spectrochim Acta A* 57:843–858.

Muniz, G.S.V., Mejía, C.F., Martinez, R., Auge, B., Rothard, H., Domaracka, A., and Boduch, P. (2017) Radioresistance of adenine to cosmic rays. *Astrobiology* 17:298–308.

Nowak, M.J. (1989) IR matrix isolation of nucleic acid constituents: the spectrum of monomeric thymine. *J Mol Str* 193: 35–49.

Nuevo, M., Materese, C.K., and Sandford, S.A. (2014) The photochemistry of pyrimidine in realistic astrophysical ices and the production of nucleobases. *Astrophys J* 793, doi: 10.1088/0004-637X/793/2/125.

Oba, Y., Takano, Y., Naraoka, H., Watanabe, N., and Kouchi, A. (2019) Nucleobase synthesis in interstellar ices. nature communications, 10, 4413

Oró, J. (1961) Comets and the formation of biochemical compounds on the primitive Earth. *Nature* 190:389–390.

Paranicas, C., Cooper, J.F., Garrett, H.B., Johnson, R.E., and Sturner, S.J. (2009) Europa's radiation environment and its effects on the surface. In *Europa,* edited by R.T. Pappalardo, W.B. McKinnon, and K. Khurana, University of Arizona Press, Tucson, AZ, pp 529–544.

Pilling, S., Andrade, D.P.P., do Nascimento, E.M., Marinho, R.R.T., Boechat-Roberty, H.M., de Coutinho, L.H., de Souza, G.G.B., de Castilho, R.B., Cavasso-Filho, R.L., Lago, A.F., and de Brito, A.N. (2011) Photostability of gas- and solid-phase biomolecules within dense molecular clouds due to soft X-rays. *Mon Not R Astron Soc* 411:2214–2222.

Stoks, P.G. and Schwartz, A.W. (1979) Uracil in carbonaceous meteorites. *Nature* 282:709–710.

Strazzulla, G., Cooper, J.F., Christian, E.R., and Johnson, R.E. (2003) Ion irradiation of TNOs: from the fluxes measured in space to the laboratory experiments. *C R Phys* 4:791–801.

Zahnle, K., Schenk, P., Levinson, H., and Dones, L. (2003) Cratering rates in the outer Solar System. *Icarus* 163:263–289.

Ziegler, J.F., Ziegler, M.D., and Biersack, J.P. (2010) SRIM—the Stopping and Range of Ions in Matter. *Nucl Instrum Methods Phys Res B* 268:1818–1823.

Address correspondence to:
Christopher K. Materese
Astrochemistry Laboratory
NASA Goddard Space Flight Center
8800 Greenbelt Rd.
Greenbelt, MD 20771

E-mail: Christopher.K.Materese@nasa.gov

Submitted 20 November 2019
Accepted 20 March 2020
Associate Editor: Lewis Dartnell